Title

Nanowire/nanotube array tandem cells for overall solar neutral water splitting

Authors

Kargar, Alireza
Khamwannah, Jirapon
Liu, Chin–Hung
et al.

Publication Date

2016

DOI

10.1016/j.nanoen.2015.11.019

Peer reviewed

Nano Energy (2016) 19, 289–296

Available online at www.sciencedirect.com

ScienceDirect

journal homepage: www.elsevier.com/locate/nanoenergy

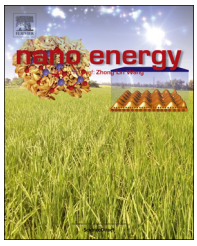

RAPID COMMUNICATION

Nanowire/nanotube array tandem cells for overall solar neutral water splitting

Alireza Kargar[a], Jirapon Khamwannah[b], Chin-Hung Liu[b], Namseok Park[a], Deli Wang[a,b,d,*], Shadi A. Dayeh[a], Sungho Jin[b,c,*]

[a]Department of Electrical and Computer Engineering, University of California-San Diego, 9500 Gilman Drive, La Jolla, CA 92093, United States
[b]Materials Science and Engineering Program, University of California-San Diego, 9500 Gilman Drive, La Jolla, CA 92093, United States
[c]Department of Mechanical and Aerospace Engineering, University of California-San Diego, 9500 Gilman Drive, La Jolla, CA 92093, United States
[d]Qualcomm Institute (QI), University of California-San Diego, 9500 Gilman Drive, La Jolla, CA 92093, United States

Received 24 October 2015; received in revised form 15 November 2015; accepted 17 November 2015
Available online 27 November 2015

KEYWORDS
Core/shell/hierarchical nanowires (csh-NWs);
Core/shell nanotubes (cs-NTs);
Photoelectrochemical (PEC) tandem cell;
Overall solar water splitting;
Neutral pH water

Abstract
In this study, we report the fabrication and characterization of a novel PEC tandem cell, consisting of p-Si/TiO_2/Fe_2O_3 core/shell/hierarchical nanowire (csh-NW) array photocathode and TiO_2/TiO_2 core/shell nanotube (cs-NT) array photoanode, for overall solar water splitting in a neutral pH water. The p-Si/n-TiO_2/n-Fe_2O_3 csh-NWs, made mainly by solution-processed methods, offer significantly improved performance in the neutral pH water with a low (positive) onset potential and photoactivity at zero bias, due to the increased reaction surface area, effective energy band alignment among p-Si, n-TiO_2 and n-Fe_2O_3 enhancing the charge separation, improved optical absorption, and enhanced gas evolution. Nitrogen modification (annealing under N_2) is used to further enhance the csh-NWs photocathodic performance. The PEC tandem cell is then able to handle overall solar water splitting in the neutral pH water with a solar-to-hydrogen (STH) efficiency of ~0.18%. The achieved results demonstrate initial steps toward the realization of full PEC devices using earth-abundant materials for solar hydrogen generation suggesting competitive performance when solar matched photoanode core material and co-catalysts are used.

*Corresponding authors at: Materials Science and Engineering Program, University of California-San Diego, 9500 Gilman Drive, La Jolla, CA 92093, United States.
E-mail addresses: d.w.wang@ieee.org (D. Wang), jin@ucsd.edu (S. Jin).

http://dx.doi.org/10.1016/j.nanoen.2015.11.019
2211-2855/

Introduction

Photoelectrochemical (PEC) hydrogen production through solar water splitting is considered as a promising approach for clean hydrogen fuel generation [1-8], which has potential for high solar-to-hydrogen (STH) efficiencies of over 30% [9]. Obtaining a PEC tandem cell (full PEC device/system) in a Z-scheme configuration to handle efficient and durable overall spontaneous solar water splitting is challenging. Its key difficulties remain in the design and engineering of efficient and stable photoelectrodes (photocathode and photoanode) using earth-abundant materials with cost-effective, simple, and scalable fabrication processes without co-integration of photovoltaic/catalysts cells or the use of conventional metal counter electrodes [10]. To run overall solar water splitting in a full PEC device, both individual photocathode and photoanode should provide a low onset potential in one specific electrolyte in a way that their photocurrents cross each other [1]. There has been tremendous progress on individual photoelectrodes with high cathodic or anodic performances [2,7,11-24], however, coupling of most of such photoelectrodes to build a PEC tandem cell has been difficult due to some limitations such as operation of photoelectrodes in different electrolytes, high onset potentials that prevent the crossing of photocurrents, etc. Indeed, Mor *et al*. have demonstrated metal oxide nanotube arrays for self-biased hydrogen generation cell, in which the correspondent photocathode and photoanode were immersed in 0.1 M Na_2HPO_4 and 1 M KOH, respectively, achieving a photoconversion efficiency of 0.30% [25].

Si/metal-oxide heterojunction electrodes have shown promising PEC performances for both cathodic and anodic conditions exhibiting potential to reduce their onset potential to the desirable values [18,26-32]. For example for the Si/Fe_2O_3 electrodes, Mayer et al. have shown the reduction of photoanodic turn-on potential through the dual-absorber nature of the n-Si/n-Fe_2O_3 junction [18], while Jun *et al*. have reported the photoanodic onset potential decrease due to the catalytic effect of n-Fe_2O_3 on n-Si [33]. Building full PEC systems based on nanowire (NW) heterojunction photoelectrodes is a promising approach for solar hydrogen production due to unique characteristics of NWs, facile NW fabrication methods, ability to form different NW heterostructures, etc. Liu et al. have reported an integrated system of catalyst-loaded Si and TiO_2 NWs for direct solar water splitting achieving a 0.12% solar-to-fuel efficiency in 0.5 M H_2SO_4 solution [4]. On the other hand, having a PEC tandem cell working in neutral pH water is highly desirable as the natural water resources such as seawater are usually in a neutral condition, and are abundant and easily disposable. Employing a neutral electrolyte for solar water splitting also prevents the undesirable use of strong acids or bases, which can lead to environmental and handling issues.

In this paper, we demonstrate a novel PEC tandem cell, consisting of p-$Si/TiO_2/Fe_2O_3$ core/shell/hierarchical nanowire (csh-NW) array photocathode and TiO_2/TiO_2 core/shell nanotube (cs-NT) array photoanode, for overall solar water splitting in a neutral pH water. The csh-NWs, made mainly by solution-processed methods, provide considerably enhanced performance in the neutral pH water with a low (positive) onset potential and photoactivity at zero bias. The csh-NWs photocathodic performance is further improved using nitrogen modification. The cs-NTs also offer improved performance. The mechanism of performance improvement for the photoelectrodes is studied. The PEC tandem cell is able to drive overall solar neutral water splitting with a STH efficiency of ~0.18%.

Experimental section

Fabrication of p-$Si/TiO_2/Fe_2O_3$ csh-NWs photocathodes

Wafer-scale vertically ordered Si NW arrays on p-type boron-doped Si(100) wafers with resistivity of 1-20 Ω cm were achieved using an aqueous Ag-assisted electroless etching technique [34]. The etching time was 20 min resulting in a NW length of ~6.5 μm. The etched Si NW samples were then dipped into buffered oxide etch (BOE) solution for 10 s to remove the native oxide layer, rinsed with deionized (DI) water, dried with N_2 gas, and transferred to atomic layer deposition (ALD) chamber (Beneq TFS 200). A thin TiO_2 shell, working as a seeding layer for the Fe_2O_3 nanorods (NRs) growth, was then deposited on the Si NW substrates using ALD deposition in thermal mode (thermal ALD) at a temperature of 250 °C. The number of cycles was 568 giving a thickness of ~25 nm on flat Si substrate based on a growth rate of 0.44 Å/cycle on Si(100) film substrate. The Fe_2O_3 NRs were finally grown on the TiO_2-coated Si NW trunks using a hydrothermal growth technique [35,36]. Briefly, akaganeite (β-FeOOH) NRs were first grown on the TiO_2-coated Si NW cores by immersing the sample in a 45 mL sealed Teflon autoclave containing a 30 mL aqueous solution consisting of 0.15 M $FeCl_3 \cdot 6H_2O$ (Iron(III) chloride hexahydrate) (Sigma-Aldrich, ≥ 99%) and 1 M $NaNO_3$ (sodium nitrate) (Sigma-Aldrich, ≥ 99.0%). The DI water resistivity and solution pH were 17.6-17.7 MΩ-cm and ~1.44, respectively. The hydrothermal reaction was carried out at a temperature of ~106 °C for 3 h. The sample was then rinsed cautiously with DI water to remove the residues and dried with N_2 gas. Lastly, the Si/TiO_2/FeOOH csh-NWs substrates were annealed at 450 °C in air (denoted as $Si/TiO_2/A\text{-}Fe_2O_3$ csh-NWs) or under N_2 atmosphere (denoted as $Si/TiO_2/N\text{-}Fe_2O_3$ csh-NWs) for 1 h. The N_2 flow during the annealing was 1000 scc/min. The growth of A-Fe_2O_3 and N-Fe_2O_3 NRs on fluorine-doped tin oxide (FTO) substrates was also performed in the same way as that mentioned for the csh-NWs samples. Before the growth, the FTO substrate was cleaned consecutively by sonication in acetone, isopropanol, and DI water for 5 min each and finally rinsed with DI water and dried with N_2 flow.

Fabrication of p-Si/TiO_2 core/shell NWs (cs-NWs) samples

The cleaned Si NW samples (discussed above) were transferred to the ALD machine to deposit a thin TiO_2 shell using the thermal ALD at a temperature of 300 °C (Figures. S6 and S7). The number of cycles was 682 giving a thickness of ~30 nm on the Si film substrate. Note that the ALD growth rate is a little larger (not significant) at higher temperature

of 300 °C, but we considered the same rate to calculate the thickness. For the N_2 annealed cs-NW samples, they were annealed at a temperature of 450 °C for 1 h under a N_2 flow of 1000 scc/min, similar condition to that mentioned for the $Si/TiO_2/N\text{-}Fe_2O_3$ csh-NWs.

Fabrication of TiO_2/TiO_2 cs-NTs photoanodes

Highly ordered TiO_2 NT arrays were prepared by an anodization process in a two-electrode electrochemical bath. Ti foil (99.5% purity, 0.25 mm thick, Alfa Aesar) and Ti mesh (80 mesh woven from 0.13 mm dia wire, Alfa Aesar) (working electrode (WE)) were cleaned in a mild detergent, rinsed with DI water and ultra-sonicated in acetone and ethanol for 5 min in each solvent. Then, the Ti foil/Ti mesh was immersed in 1:18:81 $HF:HNO_3:H_2O$ (volume ratio) for 2 min, rinsed generously with DI water and ultra-sonicated in DI water for another 5 min. They were then dried by N_2 gas flow. A Pt foil was used as the counter electrode (CE). The voltage was applied by a DC power supply (Agilent, E3612A). A thin TiO_2 NT array layer was produced by anodizing the Ti foil/Ti mesh in a solution of ethylene glycol (99.8%, JT Baker), containing 0.30% ammonium fluoride (NH_4F, 96%, Alfa Aesar) and 5% H_2, for 3.5 h at 60 V. A thin TiO_2 shell was finally deposited on the TiO_2 NTs using the thermal ALD at a temperature of 300 °C for 454 cycle numbers providing a thickness of ~20 nm on the flat Si substrate.

Characterization

The samples morphology was examined on a Philips XL30 field-emission environmental scanning electron microscope (ESEM) at an accelerating voltage of 10.0 kV. Energy-dispersive X-ray spectroscopy (EDS) and elemental mapping analyses were used to examine the materials composition. Crystal structures of samples were characterized using X-ray diffraction (XRD) by a Bruker D2 Phaser X-ray diffractometer with Cu Kα (λ=0.154 nm) as the radiation source.

PEC and IPCE measurements

To evaluate the samples performance, they were bonded to coated Cu wire at the back using indium. For the Ti substrates, indium was also used to provide ohmic contact to Ti. The edges and backside of samples were sealed using Hysol 1 C epoxy. For the mesh samples, only the contact area and edges were covered with epoxy. Current density measurements were performed in an aqueous solution of 0.25 M Na_2SO_4 buffered at pH=7.25 or 7.1 with Phosphate Buffered Saline (PBS, Sigma) (DI water resistivity was 17.6-17.7 or 18.2 MΩ-cm for pH=7.25 or 7.1, respectively) (neutral pH water) with a three- or two-electrode setup. The three-electrode setup includes sample as working electrode (WE), Pt mesh/foil as counterelectrode (CE), and Ag/AgCl (1 M KCl) as reference electrode (RE). The two-electrode setup consists of sample as WE and Pt mesh/foil as CE. A light power intensity of 100 mW/cm^2 was tuned at the samples position using a Newport solar simulator with a xenon lamp equipped with a 1.5 AM filter. The current density measurements were collected using a Digi-Ivy potentiostat. A scan rate of 10 mV/s was used for the current density measurements (linear sweep voltammetry (LSV)). During the current density measurements, a mild agitation was employed and the electrolyte was constantly purged with a small flow of N_2 gas. The applied potentials versus Ag/AgCl RE were converted to the potentials versus reversible hydrogen electrode (RHE) or normal hydrogen electrode (NHE) using the Nernst equation. The current densities here are calculated using the geometric areas. To test the full PEC system, consisting of the csh-NWs photocathode (set as WE) and the cs-NTs photoanode (set as CE) in a two-electrode setup, samples were put next to each other in a way that solar simulator can shine both samples. A monochromator (iHR 550) equipped with the solar simulator with the 1.5 AM filter as the light source was used to carry out the spectral photoresponse and incident photon-to-current efficiency (IPCE) measurements. The monochromatic light spectrum was calibrated by a silicon photodiode (Newport 818-UV). Spectral photoresponse and IPCE measurements were performed in the same three-electrode setup and electrolyte (0.25 M Na_2SO_4 buffered at pH=7.25) as used for the current density measurements with N_2 purging but without using agitation during the tests.

The solar-to-hydrogen (STH) efficiency is calculated using below equation considering 100% faradaic efficiency [1,37];

$$\eta_{STH}(\%) = \frac{100 J_{op}(1.23\ V)}{P_{in}} \quad (1)$$

where J_{op} is the photocurrent density of crossing point between photocurrents of photocathode and photoanode, and P_{in} is the incident light power density (mW/cm^2) (which is 100 mW/cm^2 here). Note that we ignored any light attenuation, which may come from the PEC setup, resulting in not having exact 100 mW/cm^2 on the sample surface. For the PEC tandem cell (full PEC system), J_{op} is the photocurrent density at zero bias (short-circuit photocurrent density).

Results and discussion

Figure 1 shows a schematic representation of fabrication procedure for the photoelectrodes. Wafer-scale vertically ordered p-Si NW arrays/cores using p-Si(100) wafer were first fabricated using an aqueous Ag-assisted electroless etching method, followed by coating of a thin ALD TiO_2 layer served as a seeding layer for the β-FeOOH NRs growth, and finally β-FeOOH NRs were grown on the TiO_2-coated Si NW backbones using hydrothermal growth method. The β-FeOOH NRs were subsequently converted into the α-Fe_2O_3 NRs by annealing the samples at 450 °C in air (denoted as A-Fe_2O_3) or under N_2 atmosphere (denoted as N-Fe_2O_3) for 1 h. The fabricated 3D array structure is denoted as p-Si/TiO_2/A-Fe_2O_3 and p-Si/TiO_2/N-Fe_2O_3 csh-NWs for annealing in air and under N_2 environment, respectively. Highly ordered TiO_2 NT arrays on Ti foil/mesh were prepared by an anodization process and subsequently, the TiO_2 NTs were coated with a thin ALD TiO_2 layer to form TiO_2/TiO_2 cs-NTs. A PEC tandem cell was made using the csh-NWs as photocathode and the cs-NTs as photoanode.

Figure 2a-d shows scanning electron microscopy (SEM) images of p-Si/TiO_2/A-Fe_2O_3 csh-NWs. The Fe_2O_3 NRs are

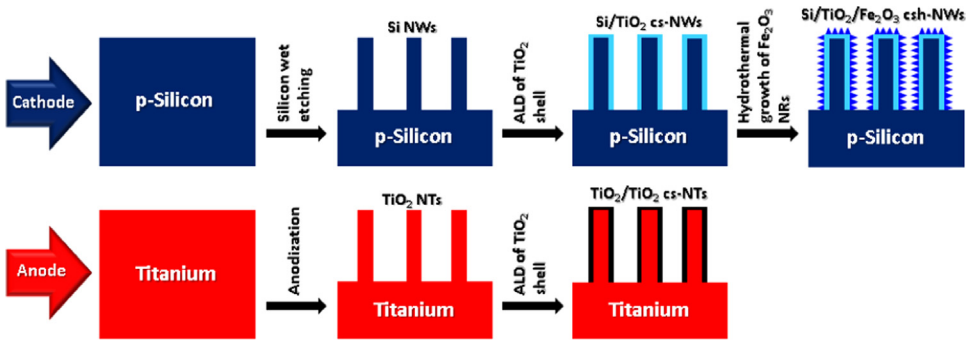

Figure 1 Schematic representation of fabrication procedure for the csh-NWs photocathode (top row) and the cs-NTs photoanode (bottom row).

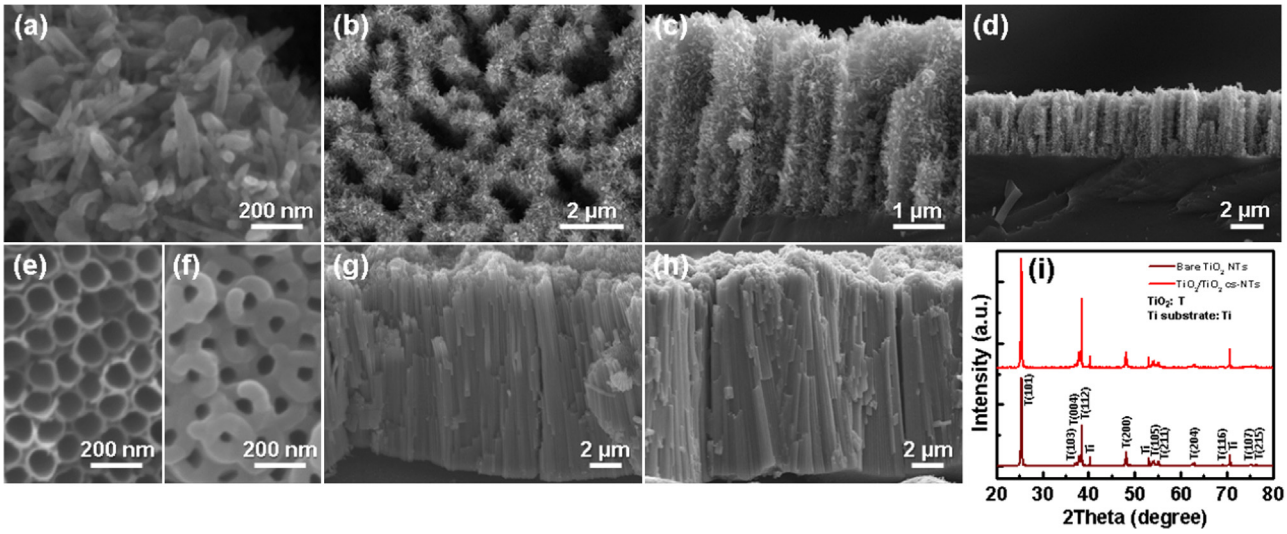

Figure 2 (a,b) Top-view (different magnification) and (c,d) cross-sectional view (different magnification) SEM images of p-Si/TiO_2/A-Fe_2O_3 csh-NW array. Top-view SEM images of (e) bare TiO_2 NTs and (f) TiO_2/TiO_2 cs-NTs. Tilted cross-sectional SEM images of (g) bare TiO_2 NTs and (h) TiO_2/TiO_2 cs-NTs. Note that the tilted angle for (g) and (h) is not the same. (i) XRD patterns of bare TiO_2 NTs and TiO_2/TiO_2 cs-NTs. All TiO_2 NTs here are from those grown on Ti foil.

polycrystalline (Figure 2a). Figure 2b shows that there are spaces between the csh-NWs, coming from good spaces between the etched Si NW cores (see Figure S1), in which water molecules can easily penetrate for water splitting reaction on the surface of csh-NWs. As shown in Figure 2c, the growth of Fe_2O_3 NRs is uniform through the entire length of tall Si NW backbones with ~6.5 μm length (Figure S1) due to uniform coverage of ALD TiO_2 layer. The csh-NWs growth is also uniform within the whole area of samples (which can be evident by the low-magnification image in Figure 2d) revealing the potential of scaling up the electrodes. Note that we did not observe any significant morphological difference in the csh-NWs with A-Fe_2O_3 and N-Fe_2O_3 NRs suggesting that the N_2 atmosphere did not significantly change the csh-NWs morphology. Also p-Si/TiO_2/A-Fe_2O_3 and p-Si/TiO_2/N-Fe_2O_3 csh-NWs showed similar XRD pattern indicating that there is no difference in their crystal structure. The A-Fe_2O_3 and N-Fe_2O_3 NRs grown directly on FTO substrate exhibit similar red color (see Figure S2), evident of successful transformation of β-FeOOH to α-Fe_2O_3 for both cases, and this was also confirmed with the same XRD pattern for both samples. The Si NW cores in the p-Si/TiO_2/A-Fe_2O_3 csh-NWs cannot be oxidized during the annealing process under air because the TiO_2 seeding layer is totally uniform (see Supporting information) and transmission electron microscopy (TEM) characterization on a similar NW structure has shown no evidence of Si NW oxidation [38]. Elemental mapping analysis shown in Figure S3 confirms the materials composition of the csh-NWs.

Figure 2e–h exhibits the SEM images of bare TiO_2 NTs and TiO_2/TiO_2 cs-NTs with an average top inner diameter of 97 nm and 57 nm, respectively. The TiO_2 shell can cover the entire length of long TiO_2 NTs (see Figure 2g and h) due to gas phase nature of ALD deposition. However, from the SEM images, it was hard to realize uniform coating of ALD TiO_2 for both inner and outer sidewalls of NTs along the whole NTs length. The XRD analyses (Figure 2i) show similar patterns for both bare TiO_2 NTs and TiO_2/TiO_2 cs-NTs revealing that both core and shell exhibit similar phase of anatase.

Figure 3a shows the current density of bare p-Si NWs, p-Si/TiO_2/A-Fe_2O_3 csh-NWs, and p-Si/TiO_2/N-Fe_2O_3 csh-NWs using a three-electrode setup in which all the samples show photocathodic behavior and there is no significant photoanodic current even at high biasing potentials of over

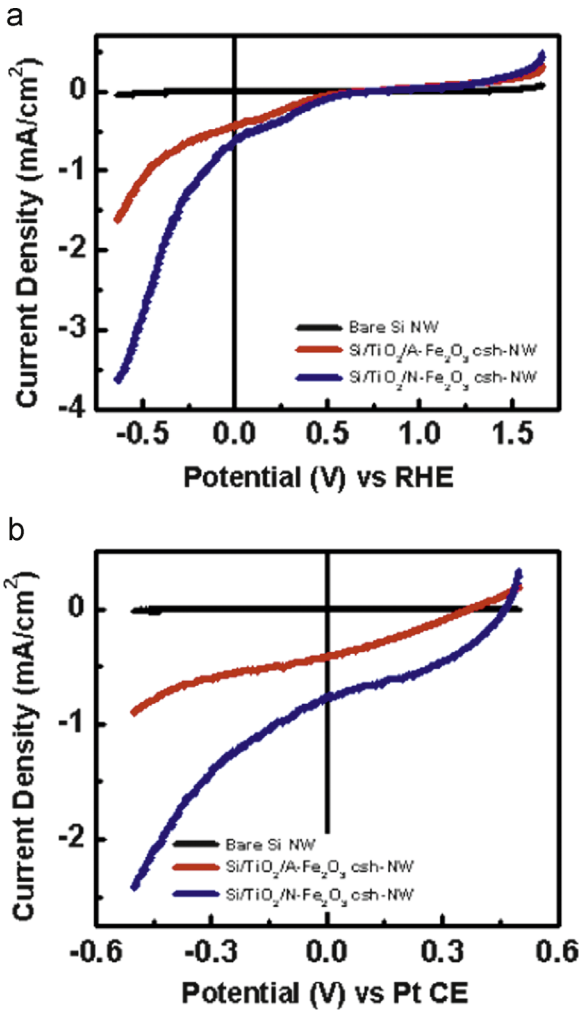

Figure 3 Current density under illumination of bare p-Si NW, p-Si/TiO_2/A-Fe_2O_3 csh-NW, and p-Si/TiO_2/N-Fe_2O_3 csh-NW arrays measured in the neutral pH water using (a) a three-electrode and (b) a two-electrode PEC setups.

+1.5 V versus RHE. The p-Si/TiO_2/A-Fe_2O_3 csh-NWs offer much higher photocathodic current and significant onset potential shift toward positive potentials compared to the bare p-Si NWs, leading to an onset potential of about +0.38 V versus RHE, a photocurrent of about −0.4 mA/cm^2 at 0 V versus RHE (see Figure 3a), and a photocurrent of about −0.43 mA/cm^2 at the water reduction potential (see Figure S4). Note that the onset potential is calculated when the net photocurrent (light current - dark current) reaches a value of −0.1 mA/cm^2. The significantly enhanced photocathodic performance is attributed to the increased reaction surface area which is evident from the SEM images, effective energy band alignment among p-Si, n-TiO_2 and n-Fe_2O_3 enhancing the charge separation (see Figure S5), improved optical absorption [18,36], and increased gas evolution coming from the 1D nature of our Fe_2O_3 NRs [39]. The morphology and PEC performance of p-Si/TiO_2 cs-NWs are shown in Figures. S6 and S7 revealing the uniform coating of ALD TiO_2 shell and its contribution in the enhanced performance. It is worth noting that the stability of the Fe_2O_3-coated p-Si photocathodes has been investigated elsewhere to rule out effect from Fe_2O_3 dissolution which may contribute to the *J-V* measurements [38]. The csh-NWs performance further improves by N_2 annealing (using N-Fe_2O_3 instead of A-Fe_2O_3) resulting in an onset potential of about +0.46 V versus RHE, a photocurrent of about −0.55 mA/cm^2 at 0 V versus RHE (see Figure 3a), and a photocurrent of about −0.61 mA/cm^2 at the water reduction potential (see Figure S4). The performance improvement can be mainly due to superior conductivity of Fe_2O_3 NRs [40,41] resulting in an enhanced collection efficiency of photoexcited electrons. Annealing under N_2 atmosphere can also enhance the conductivity of TiO_2 seeding layer assisting the performance enhancement (see Figure S7). However, annealing at 450 °C under the applied N_2 atmosphere condition may not change appreciably the band gap of Fe_2O_3 (as can be deduced from the optical images in Figure S2) or TiO_2 (no noticeable color change was observed after annealing). The N-Fe_2O_3 NRs grown on the FTO substrate also showed improved photoanodic performance than A-Fe_2O_3 NRs (data not shown here) further confirming the improved conductivity which is consistent with the reported observation elsewhere [40]. The current density measurements of the corresponding samples using a two-electrode PEC setup in Figure 3b exhibit similar trend for photocurrents as that observed with a three-electrode setup in Figure 3a. The p-Si/TiO_2/N-Fe_2O_3 csh-NWs also exhibit high IPCEs in a wide range (see Figure S8).

The achieved performance facilitates to obtain a full PEC device for overall spontaneous solar water splitting in the neutral pH water. To make the PEC tandem cell for overall solar water splitting, we used TiO_2 NT array as a model for the photoanode since it can provide a low onset potential. However, the bare TiO_2 NT sample cannot provide a high photoanodic current due to TiO_2 poor properties [42,43], and its onset potential needs to be further reduced. The TiO_2 NTs were then coated with a thin ALD TiO_2 layer forming TiO_2/TiO_2 cs-NTs to achieve a higher photoanodic current (data not shown here). The enhanced photoanodic current can be due to passivation of surface states [44,45] and improved reaction surface area. The surface of ALD TiO_2 coating is not smooth (see Figure S9) meaning that the shell coating provides more junction area. As mentioned above, both TiO_2 core and shell are anatase phase, thus there is no junction barrier between core and shell to block the charge transfer. The photoanodic current of the TiO_2/TiO_2 cs-NTs grown on Ti foil in the neutral pH water is shown in Figure 4a along with the photocathodic current of p-Si/TiO_2/N-Fe_2O_3 csh-NWs to determine the crossing point between the *J-V* curves. The photocurrents intersection is at ~0.42 V versus RHE with a photocurrent density of ~0.17 mA/cm^2, resulting in a STH efficiency of ~0.21%. Using TiO_2/TiO_2 cs-NTs grown on Ti mesh instead of Ti foil, the photoanodic performance improves (Figure 4a inset) in which the photocurrents cross each other at ~0.3 V versus RHE with a photocurrent density of ~0.3 mA/cm^2 leading to a STH efficiency of ~0.37%, due to enhanced reaction surface area coming from the mesh substrate. To illuminate both sides of the mesh sample during the current density measurement, the glass PEC cell was covered with a piece of aluminum foil.

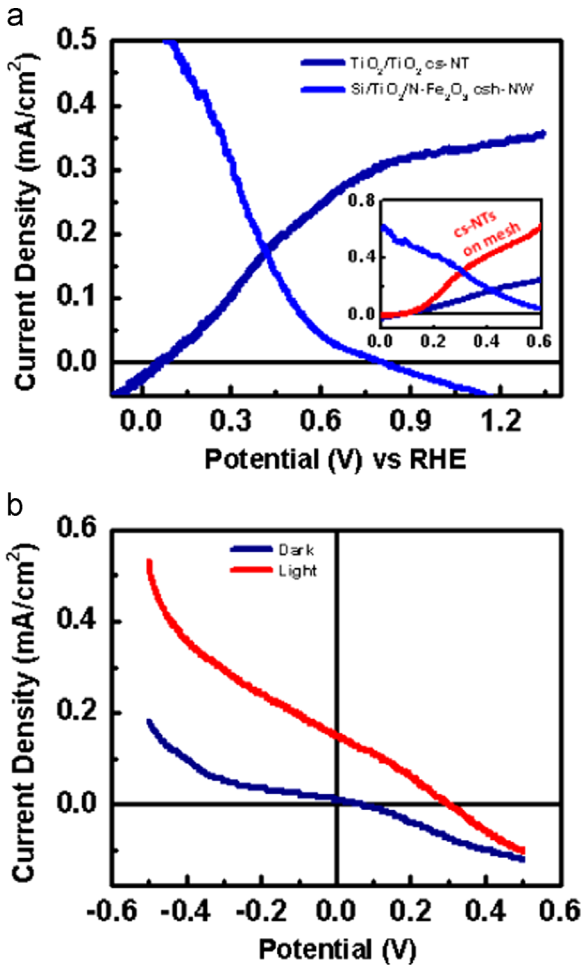

Figure 4 (a) Current density under illumination of TiO_2/TiO_2 cs-NTs (grown on foil) photoanode along with the current density under illumination of p-Si/TiO_2/N-Fe_2O_3 csh-NWs photocathode measured in the neutral pH water. Note that in this figure, the absolute value of current density for the csh-NWs is plotted. Inset shows the zoomed-in currents of the corresponding samples along with the current density under illumination of TiO_2/TiO_2 cs-NTs grown on mesh. (b) Current density at dark and under illumination of full PEC system, consisting of csh-NWs photocathode and TiO_2/TiO_2 cs-NTs (grown on foil) photoanode, tested in the neutral pH water.

The achieved performances reveal the fact that the developed photoelectrodes can run overall solar water splitting. To figure out this feasibility, a full PEC system made of these two photoelectrodes were tested in a way that the csh-NWs photocathode was set as WE and the cs-NTs (grown on Ti foil) photoanode was set as CE in a two-electrode setup. The current density of full system is shown in Figure 4b exhibiting the operation of full system in the neutral pH water with a non-zero photocurrent density of $\sim$0.15 mA/cm^2 at zero bias, which leads to a STH efficiency of $\sim$0.18%. Note that the photocurrent density of full system at zero bias ($\sim$0.15 mA/cm^2) is a little smaller than the photocurrent density at the crossing point ($\sim$0.17 mA/cm^2) which results in a slightly lower efficiency. The obtained performance is promising considering several factors; (i) performance was assessed in a neutral solution with a low morality of 0.25, (ii) all photoelectrodes were fabricated using earth-abundant materials with cheap fabrication processes except for ALD which may be replaced with another fabrication technique, and (iii) there is no catalyst loaded on the electrodes. To obtain a high STH efficiency in such a full system, a catalyst (preferably bifunctional) working in neutral or near-neutral pH water toward basic solution such as NiO [36,46,47] can be added to both photoelectrodes. Additionally, a different or composite photoanode material whose absorption is matched to the solar spectrum, has a low onset potential, and is stable can be used to substantially improve the STH efficiency beyond that achieved in this study.

Conclusions

In summary, we demonstrated the fabrication and characterization of a novel PEC tandem cell, consisting of p-Si/TiO_2/Fe_2O_3 csh-NW array photocathode and TiO_2/TiO_2 cs-NT array photoanode, for overall solar water splitting in the neutral pH water. The csh-NWs, made mostly from solution growth methods, exhibited considerably improved photocathodic performance in the neutral pH water with positive onset potentials of about +0.38 V and +0.46 V versus RHE, and photocurrents of about -0.4 mA/cm^2 and -0.55 mA/cm^2 at 0 V versus RHE for the unmodified and N-modified Fe_2O_3 NRs, respectively. The PEC tandem cell was finally shown to handle overall solar neutral water splitting with a STH efficiency of $\sim$0.18%. The obtained results reveal promising potential of making PEC tandem cells using earth-abundant materials with low cost processes for solar hydrogen fuel production.

Acknowledgments

This work was supported by the National Science Foundation (NSF CBET1236155) and the Iwama Endowed Fund at UCSD. A.K. thanks UCSD Nano3 cleanroom personnel for their support and assistance.

Appendix A. Supplementary material

Supplementary data associated with this article can be found in the online version at http://dx.doi.org/10.1016/j.nanoen.2015.11.019.

References

[1] M.G. Walter, E.L. Warren, J.R. McKone, S.W. Boettcher, Q. Mi, E.A. Santori, et al., Chem. Rev. 110 (2010) 6446–6473.
[2] M.J. Kenney, M. Gong, Y. Li, J.Z. Wu, J. Feng, M. Lanza, et al., Science 342 (2013) 836–840.
[3] S.Y. Reece, J.A. Hamel, K. Sung, T.D. Jarvi, A.J. Esswein J.J.H. Pijpers, et al., Science 334 (2011) 645–648.
[4] C. Liu, J. Tang, H.M. Chen, B. Liu, P. Yang, Nano Lett. 13 (2013) 2989–2992.
[5] O. Khaselev, J.A. Turner, Science 280 (1998) 425–427.
[6] J. Luo, J.-H. Im, M.T. Mayer, M. Schreier, M.K. Nazeeruddin, N.-G. Park, et al., Science 345 (2014) 1593–1596.

[7] G. Wang, H. Wang, Y. Ling, Y. Tang, X. Yang, R.C. Fitzmorris, et al., Nano Lett. 11 (2011) 3026–3033.
[8] X. Shi, K. Zhang, K. Shin, M. Ma, J. Kwon, I.T. Choi, et al., Nano Energy 13 (2015) 182–191.
[9] S. Hu, C. Xiang, S. Haussener, A.D. Berger, N.S. Lewis, Energy Environ. Sci. 6 (2013) 2984–2993.
[10] J.W. Ager, M. Shaner, K. Walczak, I.D. Sharp, S. Ardo, Energy Environ. Sci. 8 (2015) 2811–2824.
[11] S. Hu, M.R. Shaner, J.A. Beardslee, M. Lichterman B.S. Brunschwig, N.S. Lewis, Science 344 (2014) 1005–1009.
[12] Y.W. Chen, J.D. Prange, S. Dühnen, Y. Park, M. Gunji C.E.D. Chidsey, et al., Nat. Mater. 10 (2011) 539–544.
[13] A. Paracchino, V. Laporte, K. Sivula, M. Grätzel, E. Thimsen, Nat. Mater. 10 (2011) 456–461.
[14] M.H. Lee, K. Takei, J. Zhang, R. Kapadia, M. Zheng, Y.-Z. Chen, et al., Angew. Chem. Int. Ed. 124 (2012) 10918–10922.
[15] S.C. Warren, K. Voïtchovsky, H. Dotan, C.M. Leroy, M. Cornuz, F. Stellacci, et al., Nat. Mater. 12 (2013) 842–849.
[16] H.-P. Wang, K. Sun, S.Y. Noh, A. Kargar, M.-L. Tsai, M.-Y. Huang, et al., Nano Lett. 15 (2015) 2817–2824.
[17] S.W. Boettcher, J.M. Spurgeon, M.C. Putnam, E.L. Warren D.B. Turner-Evans, M.D. Kelzenberg, et al., Science 327 (2010) 185–187 185.
[18] M.T. Mayer, C. Du, D. Wang, J. Am. Chem. Soc. 134 (2012) 12406–12409.
[19] N.P. Dasgupta, C. Liu, S. Andrews, F.B. Prinz, P. Yang, J. Am. Chem. Soc. 135 (2013) 12932–12935.
[20] J.D. Benck, S.C. Lee, K.D. Fong, J. Kibsgaard, R. Sinclair T.F. Jaramillo, Adv. Energy Mater. 4 (2014) 1400739.
[21] Q. Ding, F. Meng, C.R. English, M. Cabán-Acevedo, M. J. Shearer, D. Liang, et al., J. Am. Chem. Soc. 136 (2014) 8504–8507.
[22] S. Chandrasekaran, T. Nann, N.H. Voelcker, Nano Energy 17 (2015) 308–322.
[23] X.-Q. Bao, D.Y. Petrovykh, P. Alpuim, D.G. Stroppa, N. Guldris, H. Fonseca, et al., Nano Energy 16 (2015) 130–142.
[24] T. Zhu, M.N. Chong, Nano Energy 12 (2015) 347–373.
[25] G.K. Mor, O.K. Varghese, R.H.T. Wilke, S. Sharma, K. Shankar, T.J. Latempa, et al., Nano Lett. 8 (2008) 1906–1911.
[26] Y.J. Hwang, A. Boukai, P. Yang, Nano Lett. 9 (2008) 410–415.
[27] M.R. Shaner, K.T. Fountaine, S. Ardo, R.H. Coridan, H.A. Atwater, N.S. Lewis, Energy Environ. Sci. 7 (2014) 779–790.
[28] J. Yang, K. Walczak, E. Anzenberg, F.M. Toma, G. Yuan, J. Beeman, et al., J. Am. Chem. Soc. 136 (2014) 6191–6194.
[29] J. Shi, Y. Hara, C. Sun, M.A. Anderson, X. Wang, Nano Lett. 11 (2011) 3413–3419.
[30] A. Kargar, K. Sun, Y. Jing, C. Choi, H. Jeong, Y. Zhou, et al., Nano Lett. 13 (2013) 3017–3022.
[31] X. Wang, K.-Q. Peng, Y. Hu, F.-Q. Zhang, B. Hu, L. Li, et al., Nano Lett. 14 (2014) 18–23.
[32] S.Y. Noh, K. Sun, C. Choi, M. Niu, M. Yang, K. Xu, et al., Nano Energy 2 (2013) 351–360.
[33] K. Jun, Y.S. Lee, T. Buonassisi, J.M. Jacobson, Angew. Chem. Int. Ed. 51 (2012) 423–427.
[34] A. Kargar, K. Sun, S.J. Kim, D. Lu, Y. Jing, Z. Liu, et al., Phys. Status Solidi A 210 (2013) 2561–2568.
[35] L. Vayssieres, N. Beermann, S.-E. Lindquist, A. Hagfeldt, Chem. Mater. 13 (2001) 233–235.
[36] A. Kargar, J.S. Cheung, C.-H. Liu, T.K. Kim, C.T. Riley, S. Shen, et al., Nanoscale 7 (2015) 4900–4905.
[37] Z. Chen, T.F. Jaramillo, T.G. Deutsch, A. Kleiman-Shwarsctein, A.J. Forman, N. Gaillard, et al., J. Mater. Res. 25 (2010) 3–16.
[38] A. Kargar, S.J. Kim, P. Allameh, C. Choi, N. Park, H. Jeong, et al., Adv. Funct. Mater. 25 (2015) 2609–2615.
[39] K. Sun, Y. Jing, C. Li, X. Zhang, R. Aguinaldo, A. Kargar, et al., Nanoscale 4 (2012) 1515–1521.
[40] Y. Ling, G. Wang, J. Reddy, C. Wang, J.Z. Zhang, Y. Li, Angew. Chem. Int. Ed. 51 (2012) 4074–4079.
[41] X. Lu, Y. Zeng, M. Yu, T. Zhai, C. Liang, S. Xie, et al., Adv. Mater. 26 (2014) 3148–3155.
[42] A.L. Linsebigler, G. Lu, J.T. Yates, Chem. Rev. 95 (1995) 735–758.
[43] E. Hendry, M. Koeberg, B. O'Regan, M. Bonn, Nano Lett. 6 (2006) 755–759.
[44] F. Le Formal, N. Tetreault, M. Cornuz, T. Moehl, M. Gratzel, K. Sivula, Chem. Sci. 2 (2011) 737–743.
[45] Y.J. Hwang, C. Hahn, B. Liu, P. Yang, ACS Nano 6 (2012) 5060–5069.
[46] M. Gong, W. Zhou, M.-C. Tsai, J. Zhou, M. Guan, M.-C. Lin, et al., Nat. Commun. 5 (2014) 4695.
[47] L. Trotochaud, J.K. Ranney, K.N. Williams, S.W. Boettcher J. Am. Chem. Soc. 134 (2012) 17253–17261.

Alireza Kargar is a PhD candidate in the Electrical and Computer Engineering Department of the University of California, San Diego. He received the B.S. degree from Shiraz University, Shiraz, Iran. His current research interests are design and fabrication of different nanostructures for solar energy conversion devices with focus on solar fuel generation systems.

Jirapon Khamwannah received her PhD degree (2015) in Materials Science and Engineering from University of California, San Diego. She is currently a lecturer at Chulalongkorn University, Thailand. Her research mainly focuses on advanced nanostructure materials and 3-D structure for applications in Dye-sensitized solar cells.

Chin-Hung Liu is a Ph.D. in the Materials Science and Engineering Program at University of California, San Diego (UCSD). He obtained M.S. degree from National Tsing Hua University (Taiwan, R.O.C.) and Bachelor degree from National Cheng Kung University (Taiwan, R.O.C.). His research topics include on magnetic materials, energy materials, packaging materials and III-V semiconductors.

Namseok Park received a B.S. degree in electrical engineering from Inha University, Incheon, South Korea in 2004 and M.S. and Ph.D. degrees from the University of California, San Diego in electrical engineering (Applied Physics) in 2010 and 2015, respectively. His works included synthesis and optoelectronic devices of wide bandgap semiconducting metal oxide thin films and development of process integration of wearable Si MOSFET circuits.

Deli Wang received his B.S. in Polymer Chemistry and Ph.D. in Material Science from the University of Science and Technology of China in 1990 and the University of California at Santa Barbara in 2001, respectively. He then worked as a postdoctoral researcher at Harvard University on semiconductor nanowires and nanoelectronics. From 2004 to 2014, he was an assistant/associate professor in the Electrical and Computer Engineering department at the University of California-San Diego. Since 2014, Deli has been working at NEEM Scientific Inc., a startup company he founded. His interests include nanotechnology, sensors, optoelectronics, clean energy, and digital health.

Shadi Dayeh received his PhD in Electrical Engineering from UC San Diego in 2008 followed by postdoctoral training at Los Alamos National Laboratory. He joined the faculty of ECE at UCSD in November 2012 where he directs the Integrated Electronics and Biointerfaces Laboratory.

Dr. Sungho Jin received his Ph.D. in Materials Science & Engineering from UC Berkeley in 1974. After joining Bell Labs at Murray Hill, NJ, he carried out forefront materials research for 26 years until he joined UC San Diego in 2002. As Distinguished Professor and Iwama Endowed Chair, he also served as Director, UCSD-wide Materials Science & Engineering Program for the past 13 years. He is a member of the US National Academy of Engineering, Fellow of APS, TMS, and MRS, and Professor Emeritus of UCSD. He received various awards including John Bardeen Award and Albert-Sauveur Achievement Award.